

## Magnetic 3d adatoms on free-standing and Ni(111)-supported graphene

Florian Ellinger 

*Faculty of Physics and Center for Computational Materials Science, Universität Wien, Kolingasse 14-16/03.65, A-1090 Vienna, Austria*

Cesare Franchini

*Faculty of Physics and Center for Computational Materials Science, Universität Wien, Kolingasse 14-16/03.65, A-1090 Vienna, Austria  
and Department of Physics and Astronomy, Alma Mater Studiorum – Università di Bologna, I-40127 Bologna, Italy*

Valerio Bellini \*

*S3-Istituto di Nanoscienze-CNR, Via Campi 213/A, I-41125 Modena, Italy*



(Received 30 August 2020; revised 12 November 2020; accepted 22 December 2020; published 12 January 2021)

We present an extensive density functional theory analysis of the structural, electronic, and magnetic properties of isolated 3d transition metal adatoms (from Ti to Co) adsorbed on free-standing and Ni(111)-supported graphene. We discuss how the energetics of different adsorption sites is influenced by the filling of *d*-orbital filling across the 3d series and identify a direct correlation between the adatom-graphene distance and the degree of charge transfer. The presence of the Ni substrate is found to have stronger impact on the adatoms at the end of the series, leading to modifications of the preferred adsorption site, charge transfer, and spin properties. The magnetic exchange coupling between the spin of the adatom and the Ni magnetization changes as a function of the adatom both in sign (preferred antiferromagnetic exchange for Ti, V, and Cr, and ferromagnetic alignment for the other elements) and in magnitude (from 90 meV for Mn to  $\approx 10$  meV for Fe and Co).

DOI: [10.1103/PhysRevMaterials.5.014406](https://doi.org/10.1103/PhysRevMaterials.5.014406)

### I. INTRODUCTION

Over the last decades there has been an increasing interest in the study of single (magnetic) ions adsorbed on a variety of surfaces [1–5]. If doping effects have been at the heart of earlier investigations, intrinsic electronic and magnetic properties of the adatoms have been lately in the spotlight for, e.g., the realization of single-ion magnets (SIM) for spintronics applications. The recent observation of magnetic remanence of Ho ions on MgO(100)/Ag(100) [6] has opened new perspectives in the downsizing process of magnetic memories [5]. The ingredients behind this promising observation are (i) a proper symmetry at the adsorption site, which, by crystal field splitting, leads to energy levels which optimize orbital anisotropy, together with (ii) the presence of a nonreactive, rigid substrate which minimizes electronic screening and other possible interaction channels such as phonons.

If rare earth ions, in virtue of their large spin and orbital moment, emerge as natural candidates for the realization of SIMs, the theoretical and experimental investigations have been extended to transition metal (TM) ions, especially 3d ions, and among them Co. Among possible substrates, graphene has been set forward as the optimal scaffold where to deposit adatoms/molecules, owing this to its intrinsic electronic properties. For instance, 3d metal phthalocyanines have been investigated on graphene deposited on Ir(111) and Ru(111) (also in the presence of intercalated magnetic layers be-

low graphene), as well as on graphene/Ni(111), and magnetic coupling with the substrate magnetization was detected up to room temperature [7].

It is therefore of timely importance to investigate how electronic and magnetic properties of 3d ions behave upon adsorption on such graphene-based surfaces. Many articles, mostly theoretical, have been already devoted to the study of the 3d atom series on the graphene layer by means of density-functional theory [8–14]. Due to the atomlike character of the orbitals involved in the adatom-substrate interaction, electron correlation effects are expected to play a significant role and have been explicitly taken into account in the calculation. Cobalt adatoms on graphene have been studied in great detail by a variety of computational approaches [15–18], which have also disclosed the presence of interesting Kondo physics [19–21]. From the experimental point of view, a few measurements have been reported of TM on graphene [22–25] and other Dirac materials such as black phosphorous [26]. These studies have revealed that different absorption sites might exist, depending on the specific type of interaction between the graphene layer and the substrate. Typically, if graphene interacts with the substrate, a reduction in the number of populated adsorption sites is observed.

In some cases, if the intrinsic magnetic anisotropy of the TM ion is strong enough to stabilize a local magnetic moment, it can be used as a magnetic probe in magnetic experiments. Alternatively, one can exploit the magnetic exchange interaction between the adatom and the substrate spins. In graphene-based structures, for instance, this exchange coupling has been realized by intercalating magnetic

\*valerio.bellini@unimore.it

multilayers between graphene and a nonmagnetic substrate, or by directly employing a magnetic substrate such as Ni. As a matter of fact, the accumulated experience has elected graphene/Ni substrate as the optimal setup. The resulting magnetic coupling of hybrid TM-molecular systems with magnetic substrates has been studied in depth [27–31]. The size and sign of the coupling is found to vary, and only a thorough analysis of the spin-communication channels allows one to understand the coupling mechanism. Magnetic coupling and spin-filtering related physics between 3d transition metals through graphene have been investigated by DFT in a somewhat systematic manner only in the case of layered heterostructures [32–35], while investigations at the single adatom level have been discouraged due to the prohibitive computational effort.

In this work we aim to fill such a gap by presenting an extensive characterization of the electronic and magnetic properties of 3d-series TM ions (from Ti to Co) adsorbed on graphene/Ni(111) as well as, for comparison, on an unsupported graphene monolayer by means of density functional theory calculations. The comparison between the two substrates helps us to unravel the role of the metallic substrate in the energetics of the different adsorption sites. Moreover, we analyze magnetic exchange couplings between the 3d adatom and Ni substrate spins, and discuss trends in the properties across the 3d series in terms of *d*-band filling and of the different interactions with the substrate.

## II. METHOD

Density functional theory (DFT) calculations have been performed using the projector augmented wave (PAW) method as implemented in the VASP code [36,37] with the Perdew-Burke-Ernzerhof (PBE) exchange correlation functional [38]. A cutoff energy of 550 eV for the plane wave basis has been used. Van der Waals (vdW) dispersion interactions have also been taken into account by means of semiempirical potential DFT-D2 by Grimme [39]. Inclusion of vdW interactions in this approximation together with the GGA-PBE functional has been found to be a successful approach to describe interactions between graphene and metals [40]. On-site Coulomb corrections to the *d* orbitals of the 3d adatom have been considered using the rotationally invariant LDA + U (Local Density Approximation + U) introduced by Liechtenstein *et al.* [41]. We chose values of  $U = 3$  eV and  $J = 1$  eV, based on the observation that values of  $U = 2$  eV (for the top and bridge sites) and  $U = 4$  eV (for the hollow site) fail to reproduce the binding energy curves calculated by more accurate multideterminant methods [17]. We refer to our results obtained by this approach with the label ‘GGA + U’ (Generalized Gradient Approximation + U). We have witnessed that using this methodology, extreme care must be taken in order to reach the correct lowest energy configuration. As a matter of fact several metastable states can be achieved depending on the initialization of the starting charge density and the parameters that rule the self-consistent cycles [42]. In order to deal with this uncertainty, for each calculation a whole set of initialization is taken into account as described in Ref. [43] (see Table S1 in Ref. [43]).

Concerning the extraction of the magnetic properties, we do not include in the present calculations spin-orbit effects, and we consider all the spins to be collinear. It is well known that the tackling by DFT of noncollinear magnetism and spin-orbit coupling is a difficult task, and require the calculations of properties that converge very slowly with the parameters of the calculations, e.g., the size of the *k* mesh for Brillouin zone integration, and cannot be carried out in a large-scale systematic study as the one proposed here. Moreover, except maybe for Co, magnetic anisotropy energies in TM adatoms are expected to be at least one order of magnitude smaller than TM-Ni magnetic exchange, meaning that TM adatom spins would be collinearly pinned to the Ni magnetization. In addition, magnetic frustration induced noncollinearity is not expected in the systems under study.

The morphology of the graphene/Ni(111) interface has been investigated experimentally [44] and the most common stackings are the top-fcc and top-bridge ones. The former stacking is characterized by having two inequivalent C atoms, one on top of the Ni(111) surface atom ( $C_{\text{top}}$ ), the other on the fcc site ( $C_{\text{fcc}}$ ). In the top-bridge stacking the two C atoms are equivalent and sit in bridge positions with respect to underlying Ni atoms (see Fig. S1 in Ref. [43] for a sketch of the stackings). We find the top-fcc stacking to be more stable by 6.5 meV/C than the bridge-top one, and we will consider only this stacking in the following discussion. The simulation cell is composed of a four-monolayer thick Ni slab on top of which a single graphene layer is placed with top-fcc stacking, in similarity with the setup used in Ref. [45].

Isolated 3d adatoms are placed in a  $4 \times 4$  two-dimensional (2D) supercell with an in-plane Ni lattice constant  $a_{\text{latt}}^{\text{Ni}} = 3.49$  Å, and a vacuum region of 25 Å (to reduce the slab’s replica interaction along the *z* direction). With this setup the total number of atoms per cell amounts to 97 (64 Ni, 32 C, and the adatom). Possible adsorption sites in the case of the G/Ni(111) substrate are sketched in Fig. 2. In the case of the unsupported G substrate, only top, hollow, and bridge sites are inequivalent. A  $8 \times 8$  2D Gamma-centered *k*-point grid has been employed to sample Brillouin zone integration. Structural relaxations have been considered for the 3d adatoms, the graphene layer and the topmost Ni layer, until residual forces were smaller than 0.02 eV/Å. In the case of the adatom on unsupported graphene, the Ni atoms have been removed from the cell, while the in-plane cell and *k*-point sampling are the same as in the G/Ni substrate, and all the atoms are allowed to relax. Charge transfers were studied using the Bader analysis [46].

## III. 3d ADATOMS ON UNSUPPORTED GRAPHENE LAYER

In this section we briefly summarize the results on the adsorption of TM adatoms on the unsupported graphene monolayer, a topic that has been already addressed by DFT in several works in the last decade [8–14]. Such investigations have delved into the influence of the proposed methodology (LDA/GGA, LDA + U, Van der Waals corrections) on properties such as the preferred adsorption site, adsorption geometry, and ground-state electronic and spin configuration of the adatoms. The adatoms can be classified as physisorb or chemisorb on graphene depending on the adsorption energy

TABLE I. Collection of relative adsorption energies  $E_{\text{ad}}$  (meV), Bader charges of the TM adatom ( $e^+$ ), Ad-G distance, and spin moment  $m_d$  ( $\mu_B$ , integrated on the  $d$  orbitals using spheres of radii 2.3 Å for Ti and V, 2.2 Å for Cr and Mn, and 2.0 Å for Fe and Co) for TM adatoms on unsupported graphene at either the hollow or top site. In brackets the total cell magnetization  $M_{\text{cell}}$  ( $\mu_B$ ) is reported.

|        | Ti  | V                | Cr               | Mn               | Fe               | Co               |
|--------|---|------------------|------------------|------------------|------------------|------------------|
|        | $E_{\text{ad}}$ (meV)                                 |                  |                  |                  |                  |                  |
| Hollow | 0   | 0                | +73              | 0                | 0                | 0                |
| Top    | +181  | +192             | 0                | +15              | +138             | +46              |
|        | Bader charge ( $e^+$ )                                |                  |                  |                  |                  |                  |
| Hollow | 0.88  | 0.66             | 0.47             | 0.67             | 0.73             | 0.53             |
| Top    | 0.72  | 0.47             | 0.39             | 0.57             | 0.31             | 0.30             |
|        | Ad-G distance (Å)                                     |                  |                  |                  |                  |                  |
| Hollow | 1.88  | 1.94             | 2.17             | 2.08             | 1.53             | 1.66             |
| Top    | 2.25  | 2.31             | 2.32             | 2.24             | 2.34             | 2.10             |
|        | $m_d$ and $M_{\text{cell}}$ (in brackets) ( $\mu_B$ ) |                  |                  |                  |                  |                  |
| Hollow | +1.84<br>(+3.25)                                      | +2.77<br>(+4.25) | +3.86<br>(+5.62) | +4.25<br>(+5.75) | +2.06<br>(+2.00) | +1.78<br>(+2.25) |
| Top    | +1.81<br>(+3.16)                                      | +3.09<br>(+4.75) | +3.87<br>(+5.81) | +4.17<br>(+5.46) | +2.83<br>(+4.11) | +1.85<br>(+2.84) |

and corresponding adatom-graphene distance [15,17,47,48]. Moreover, it has been shown that there is a correlation between the electronic configuration of the adatom and its distance from the substrate. Specifically, the adatom can assume an electronic configuration with progressively larger occupation of the  $s$  shell, from  $d^{n+2}s^0$ , through  $d^{n+1}s^1$  to  $d^n s^2$ , with increasing equilibrium adatom-graphene distance. We note in passing that the free atoms attain a  $d^n s^2$  configuration for all the elements except for Cr for which a  $d^5 s^1$  is preferred. The relative stability and characteristic of a specific adatom/graphene solution depends crucially on the local coordination and therefore on the adsorption site: depopulation of the  $s$  orbital, promoting electrons in the  $d$  orbitals, is favored by adsorption on the hollow site, as compared to top and bridge sites. As discussed in Ref. [10] moving away from the hollow adsorption site the  $s$  orbital hybridizes with low-energy graphene states, thus attenuating  $p$ - $d$  bonding. One thing that should be kept in mind is that the results obtained by computer simulations are sensitive to the adopted methodology. In particular, since the spatial extent of the  $d$  orbitals is influenced by intraorbital correlation effects, different preferred adsorption sites have been found across the series depending on whether on-site Coulomb interactions have been considered or not.

We present in the following our results for the adsorption of 3d adatoms from Ti to Co on unsupported graphene (Sc and Ni atoms are not discussed since in many cases a magnetic solution was not found). We will focus on data obtained for hollow and top adsorption sites to compare thereafter with the ones of the graphene/Ni(111) substrate, for which the bridge site is not an energy minimum (see Ref. [45]).

In Table I we list the adsorption energies  $E_{\text{ad}}$  (relative to the ground-state one, set to zero), the adatom Bader charge [46], and the adatom-graphene (Ad-G, from now on) distance, as given by GGA + U. In the case of the hollow site, Ad-G refers to the difference in the  $z$  coordinates between the adatom and

the nearest-neighbor C atom (hexagon) beneath it, while for the top site it is the difference in the  $z$  coordinates between the adatom and the C atom beneath it. Note that the C atoms that bind with the adatoms are displaced, either above or below, the unperturbed graphene plane by some modest quantities ( $\leq 0.1$ – $0.2$  Å).

We first note that hollow adsorption sites are favored for all the elements with the exception of Cr, with a relative stability, compared to the top site, ranging from tens to hundreds of meVs. This is in general agreement with previously reported data, although a top adsorption site has been reported to be the ground state in GGA + U calculations of Ref. [10], where a value of  $U=4$  eV has been used. The analysis of the Bader charges indicates that for all elements in the series electrons are transferred from the adatom to the graphene layer, leaving the net charge on the adatom positive. We also note that the charge transfer is larger for hollow site geometry, in line with the larger adsorption energies observed as compared to the top site, which results in smaller (by several tenths of Å) Ad-G distances. Further analysis on the relation between the Bader charges and the TM-G distances is given in Fig. S2 [43].

Concerning the total (cell) magnetization  $M_{\text{cell}}$  and the local (integrated on the  $d$  orbitals) spin moments  $m_d$ , we observe that the former is always larger than the latter, except for Fe. This can be traced back to the occupation of the majority spin channel of the  $4s$  orbital of the adatoms, which leads to an additional contribution to the total spin moment, and, to a much lesser extent, to the induced spin polarization on the graphene layer. We also note that larger spin  $d$  moments are found for the top sites compared to the hollow sites for all the elements, except Mn. The analysis of the electronic occupation in the  $d$  and  $s$  shells of the adatoms for each spin channel, reported in Fig. S3 of Ref. [43], allows one to assign an electronic configuration close to the  $d^{n+1}s^1$  one for all the elements in general agreement with previous works. A comparison between the values of  $M_{\text{cell}}$  obtained by our methodology and previously published data is given in Fig. S4 of Ref. [43].

From the analysis of the local density of states (LDOS) at the hollow and top sites we can extract how adatom orbitals with different symmetries interact with the graphene layer. In order to not overburden the discussion, we limit the analysis to Co (displayed in Fig. 1), while similar observations can be deduced for all other elements of the series, whose LDOS are presented in Ref. [43]. First we note that for both adsorption sites the  $s$  state is represented by a spin-polarized peak, that for Co is located at the Fermi level. This orbital is spatially localized on the adatom, and contributes to the total spin of the system as discussed above. The  $d$ -projected LDOS assumes different characteristics for the two adsorption sites, leading to distinct types of interaction with the underlying C atoms. In the hollow configuration, the occupied  $d_{xz,yz}$  and  $d_{x^2-y^2,xy}$  states of the adatom are spread over a wide energy window of about 5 eVs and interact with the graphene  $\pi$  states, which span across the same energy window. The  $d_{z^2}$  states, on the other hand, are strongly localized at low energy ( $\approx 3$  eV) and do not contribute to substantial hybridization with the substrate. In the top site geometry, we observe a reversed situation where  $d_{x^2-y^2,xy}$  and  $d_{xz,yz}$  states shrink, while the  $d_{z^2}$  orbital is broader and moved to higher energy.

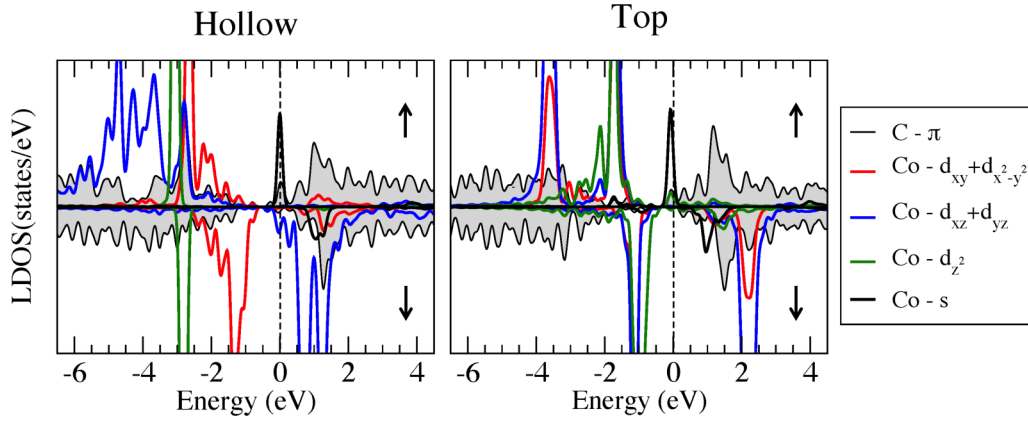


FIG. 1. Orbital- ( $s$  and  $d$ ) and spin- (majority and minority) projected local density of states (LDOS) of Co adsorbed at the hollow (left panel) and top (right panel) sites. The shaded gray curve is the spin-projected  $\pi$  state of the nearest-neighbor C atom (see text).

#### IV. 3d ADATOMS ON GRAPHENE/Ni(111)

We now move to the case where the  $3d$  adatoms are deposited on a graphene layer supported by a magnetic Ni(111) substrate.

The G/Ni(111) has been studied in the past as possible substrate [44,49] on top of which magnetic nanostructures have been deposited and characterized by theoretical and experimental approaches [27–31,50,51]. Some of us have recently [45] investigated the adsorption of Co adatoms on G/Ni(111), and in the following we extend the theoretical characterization to the  $3d$  series from Ti to Co. Similarly to Ref. [45], and following the type of analysis proposed in the previous section on free standing graphene, we have inspected all possible adsorption sites, that in case of G/Ni(111) are, by symmetry, limited to four: (a) top, (b) fcc, (c) hollow, and (d) bridge (see Fig. 2). As discussed in Ref. [45], the bridge site is not stable and upon relaxation falls back to one of the other sites, and

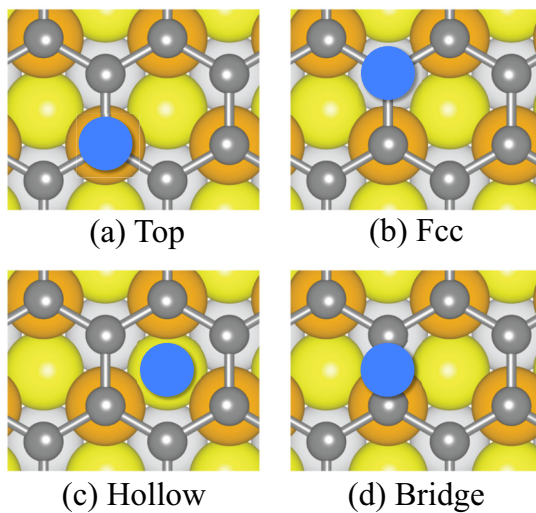


FIG. 2. Schematic view of the four different adsorption sites for the adatom/G/Ni(111) system. The blue circles identify the adatom. The small gray circles represent the graphene network. Finally, the Ni(111) substrate is displayed by large circles (orange, top layer; yellow, sub-surface layer; light gray, sub-sub-surface layer).

therefore will not be considered in the discussion. Adatoms on top and fcc sites differ on whether the adatom is on top of a C atom that, in turn, is on top or not of a Ni atom of the substrate, respectively.

Since the substrate is now magnetic, there is an additional degree of freedom, namely the sign of the coupling between the  $3d$  spin of the adatom and the magnetization of the Ni substrate. Therefore, six different solutions for each element of the  $3d$  series have been inspected, i.e., for each of the three adsorption sites both ferro- (FM) and antiferromagnetic (AFM) coupling between the adatom and Ni substrate spins were considered.

To simplify the discussion we subdivide the presentation of the structural and the magnetic data in two tables. Table II summarizes the FM/AFM average relative adsorption energies (that is, the average of the values obtained in the FM and AFM solutions), and the FM/AFM averaged Bader charge, as well as the FM/AFM averaged Ad-G distance (see the definition in the previous section). The exchange energies and spin moments are collected in Table III.

The influence of the adsorption geometry on  $E_{ad}$  is found to be larger (up to hundreds of meV) compared to the changes

TABLE II. FM/AFM averaged (see text) relative adsorption energy and Bader charges of the adatom for the adatom/G/Ni(111) system in the three considered adsorption geometries (hollow, top, and fcc).

|        | Ti   | V    | Cr   | Mn   | Fe   | Co   |
|--------|--|------|------|------|------|------|
|        | FM/AFM averaged $E_{ad}$ (meV)                 |      |      |      |      |      |
| Hollow | 0  | 0    | +172 | 0    | +100 | +287 |
| Top    | +76  | +26  | +116 | +6   | +55  | +217 |
| Fcc    | +247   | +405 | 0    | +5   | 0    | 0    |
|        | FM/AFM averaged Bader charges ( $e^+$ )        |      |      |      |      |      |
| Hollow | 0.85   | 0.74 | 0.38 | 0.59 | 0.36 | 0.43 |
| Top    | 0.80   | 0.78 | 0.38 | 0.55 | 0.28 | 0.26 |
| Fcc    | 0.60   | 0.70 | 0.37 | 0.35 | 0.29 | 0.20 |
|        | FM/AFM averaged Ad-G distance ( $\text{\AA}$ ) |      |      |      |      |      |
| Hollow | 1.91   | 1.93 | 2.26 | 2.09 | 2.08 | 1.75 |
| Top    | 2.26   | 2.18 | 2.33 | 2.25 | 2.28 | 1.99 |
| Fcc    | 2.21   | 2.25 | 2.20 | 2.33 | 2.13 | 1.99 |

TABLE III. Exchange energy ( $E_{\text{ex}}$  in eV) and adatom  $d$  spin moment ( $m_d$  in  $\mu_B$ ) for the Ad/G/Ni(111) systems, at different adsorption sites (hollow, top, fcc) in both AFM and FM spin alignment. The energies for the lowest energy adsorption sites are highlighted in bold.

|            | Ti                    | V          | Cr         | Mn         | Fe         | Co        |
|------------|-----------------------|------------|------------|------------|------------|-----------|
|            | $E_{\text{ex}}$ (meV) |            |            |            |            |           |
| Hollow     | <b>-60</b>            | <b>-68</b> | -82        | <b>+89</b> | +112       | -20       |
| Top        | +2                    | -74        | -37        | +81        | +87        | -33       |
| fcc        | -85                   | +27        | <b>-67</b> | +74        | <b>+10</b> | <b>+8</b> |
|            | $m_d$ ( $\mu_B$ )     |            |            |            |            |           |
| Hollow FM  | +1.65                 | +2.50      | +3.88      | +4.18      | +2.94      | +1.67     |
| Hollow AFM | -1.67                 | -2.79      | -3.85      | -4.25      | -2.70      | -1.78     |
| Top FM     | +1.60                 | +2.46      | +3.87      | +4.17      | +2.88      | +1.78     |
| Top AFM    | -1.70                 | -2.73      | -3.87      | -4.22      | -2.67      | -1.86     |
| fcc FM     | +1.77                 | +2.81      | +3.81      | +4.18      | +2.65      | +1.87     |
| fcc AFM    | -1.89                 | -2.65      | -3.82      | -4.37      | -2.53      | -1.81     |

induced by the spin alignment (i.e., the sign of the magnetic coupling) reported in Table III. Moreover, the effect of the Ni substrate on  $E_{\text{ad}}$  is not straightforward, and varies across the 3d series. Overall, there is a clear preference either for hollow or fcc adsorption sites depending on whether the adatom is an element at the beginning or the end of the 3d series, with some outliers in the middle of the series: Ti, V, and Mn prefer to adsorb on the hollow site, whereas Cr, Fe, and Co at fcc ones. The top site is never found to be lowest in energy for the whole 3d series. Compared to Table I, the presence of the Ni substrate modifies the ground-state adsorption site only for Fe and Co. For Mn the adsorption energies are virtually independent on the specific adsorption site with differences within 5 meV, and this holds in the presence (Table II) or absence (Table I) of the Ni substrate.

Concerning the Ad-G distances, the comparison between the data in Tables I and II shows that the presence of the Ni substrate induces mostly minor modifications to the equilibrium distances of the adatoms on graphene ( $\leq 0.1 \text{ \AA}$ ). The only major deviation ( $\approx 0.5 \text{ \AA}$ ) is found for Fe in the hollow site, that converges to a  $3d^7 4s^1$  instead of the  $3d^8 4s^0$  attained on unsupported graphene, as will be discussed below.

The adatom Bader charges given in Table II point to similar conclusions, concerning the amount of charge transfer along the 3d series, as the ones drawn for the unsupported graphene layer. To better understand the role of the substrate we plot in Fig. 3 the comparison between the adatom Bader analysis for unsupported graphene (hollow and top) and G/Ni(111) substrate (hollow and top/fcc, the latter being the value averaged over the top and fcc sites). For each adsorption site (red circles and blue squares for hollow and top/fcc, respectively), the comparison between the unsupported (open symbols) and Ni(111) supported case (filled symbols) shows that, except for V, the presence of the Ni substrate reduces the charge transfer from the adatom to the graphene (by about  $0.1 e^+$  for earlier TM and about  $0.2\text{--}0.3 e^+$  for the late members of the TM series). This is in line with the observation that the interaction between adsorbates and graphene should decrease when graphene starts to interact with the supporting substrate. This has been discussed, for

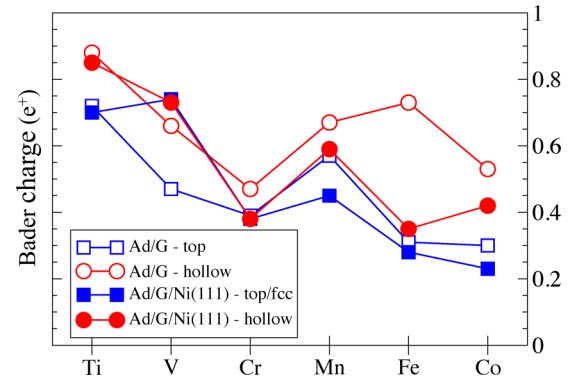


FIG. 3. Spin-coupling averaged Bader charges for the unsupported Ad/G and supported Ad/G/Ni(111) systems.

instance, by Donati *et al.* [22,25] for Co adatoms deposited on G/Ir(111), G/Pt(111), and G/Ru(0001). The relative increase of the graphene-substrate interaction (moving from a 5d to 4d metal) entails a decrease in the hybridization between the Co adatom and the graphene states (measured in terms of the degree of Ad to G charge transfer), and correspondingly to an increase in the size of the spin and orbital moments. Moreover, STM experiments observe a change in the preferred adsorption site from hollow (G/Ir and G/Pt) to top (G/Ru), and similar results have been found adsorbing TM adatoms on pristine epitaxial and quasifree standing monolayer graphene [24]. Being Ni a 3d metal, we can qualitatively place our G/Ni substrate on the far right of this “interaction ladder,” while similarly the unsupported graphene layer can be inserted on the far left, i.e., G - G/Ir - G/Pt - G/Ru - G/Ni, with increasing graphene-substrate interaction. Our result of a preferred hollow adsorption site for G and a fcc adsorption site for the G/Ni substrate for a Co adatom follows the interaction trend discussed above. Quantification of this interaction by DFT calculations in terms of graphene doping/binding energies [52] or from experiments on thermoelectric potential [53], core level photoemission spectroscopy [54], and Debye surface temperature [55] has been demonstrated. There are several aspects behind such “substrate tuning” that should be considered with special care. For instance, by changing the scaffold below graphene, depending on the lattice mismatch, flat or rippled (Moiré superlattice) graphene can be obtained [56]. In this way, within the same substrate, both low and high interacting regions can be simultaneously achieved, as is the case of G/Ru(0001) [21]. The driving mechanism in this case is the modification of the number of available states near the Fermi level, which is responsible for electronic screening in the case of Kondo physics. Most importantly, such chemical control can be achieved also in a strongly interacting substrate such as the G/Ni one, by intercalating metal layers below graphene [27,57–61]. Even defects on graphene can act as manipulators of the spin state of molecular magnetic adsorbates [62]. Therefore, the mechanisms behind the substrate-induced modification of the adsorbate-graphene interaction can be of diverse nature and offer a unique playground for the realization of tunable functional devices.

We now move to the discussion of the occupation of the adatoms 3d orbital on G/Ni(111) presented in Fig. 4 [63].

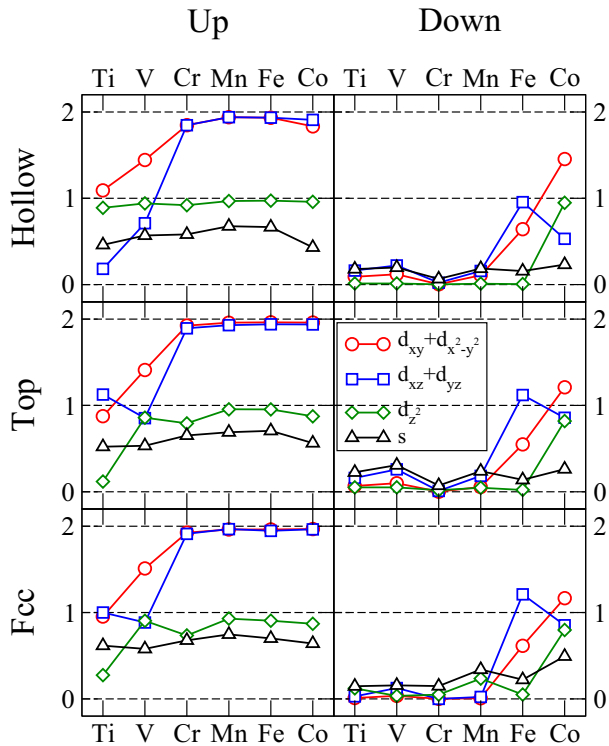


FIG. 4. Spin-decomposed (majority, Up; minority, Down) orbital occupation ( $d$  and  $s$ ) of the TM adatoms on G/Ni(111) for top, hollow, and fcc adsorption geometries. Dashed lines mark integer (one and two) occupations. Solid lines are a guide for the eye.

The overall trend follows the filling sequence obtained in the unsupported case (Fig. S3 in Ref. [43]), with some exceptions. The Fe at hollow site setup, which represents a metastable  $3d^7 4s^1$  solution without Ni(111) support, becomes the ground state for the Fe/G/Ni(111) system. We have analyzed the effect of the inclusion of vdW corrections in the bonding of the Fe adatom (see Table S2 in Ref. [43]), and they are found to be marginal. For the V at top/fcc sites, the presence of Ni induces a preferential occupation of the  $d_{z^2}$  symmetry orbital (green diamonds) at the expense of a double occupation of the  $d_{xz} + d_{yz}$  symmetry. The results for Co require some additional reasoning. For the free Co atom a nominal  $3d^7 4s^2$  occupation is expected, i.e., a value of  $n_h^d = 3$ , where  $n_h^d$  is the number of holes in the  $d$  shell. According to Donati *et al.*, a decreased Co-G hybridization is accompanied by a decrease in the  $d$  occupation of Co. Values of  $n_h^d = 1.8, 2.0,$  and  $2.5$  holes in the  $d$  orbital, respectively for G/Ir(111), G/Pt(111), and G/Ru(0001) substrates, have been extracted by the fitting of multiplet calculations to XMCD spectral lines [25]. From our data, the effect of substrate and adsorption site on the total  $d$  occupation (not shown) is rather marginal (of the order of  $0.05 e^-$ ), and no clear trend is observed. This can be traced back to the fact that Co assumes always a  $3d^8 4s^1$  electronic configuration in the ground state.

Concerning the magnetic properties we present in Table III the exchange energies  $E_{\text{ex}} = E_{\text{tot}}^{\text{AFM}} - E_{\text{tot}}^{\text{FM}}$  defined as the difference between the total energies of the ferro- and antiferromagnetic solutions, with the  $3d$  spin moment coupled parallel or antiparallel to the Ni magnetization, respectively.

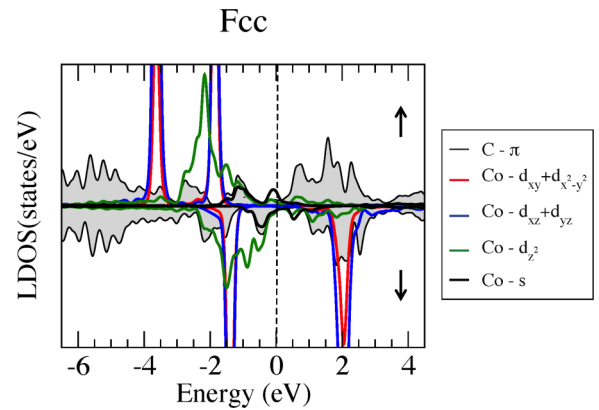


FIG. 5. Orbital- ( $s$  and  $d$ ) and spin- (majority and minority) projected local density of states (LDOS) of Co(Fcc)/G/(Ni111). The shaded gray curve is the spin-projected  $\pi$  state of the C atom beneath it.

Positive (negative) values indicate that ferro- (antiferro-) magnetic coupling is favored between the adatom and Ni substrate spins.

We note that exchange energies span from just a few to about 100 meV and vary both in size and sign for each element of the series as a function of the adsorption site. The middle members of the TM series (Cr, Mn, and Fe) exhibit exchange energies with the same sign for all the adsorption sites, whereas for the other elements site-induced spin flips are observed. The analysis of  $E_{\text{ex}}$  for each individual adsorption site does not show any clear discernible trend moving across the  $3d$  series. On the other hand, if we look at the ground-state values (highlighted in bold), defined as the exchange energies calculated for the energetically most favorable adsorption site, the coupling is predicted to be antiferromagnetic at the beginning of the series, from Ti to Cr, and ferromagnetic at the end of the series, from Mn to Co; for Fe and Co, however, absolute values of  $E_{\text{ex}}$  amount to only  $\approx 10$  meV.

To conclude the discussion of the magnetic properties, we show in the lower panel of Table III the adatom spin moments integrated over the  $d$  orbitals for both magnetic couplings, at all three adsorption sites. In line with the trend in the occupations (Fig. S3 in Ref. [43] and Fig. 3), the spin moments are similar to the ones obtained for the unsupported setup presented in Table I. At first sight the presence of the Ni substrate induces only minor modifications on the magnetic properties of the  $3d$  adatoms (see the spin densities for the hollow site reported in Fig. S5 of Ref. [43]). Variations are marginal, within 10%, except for Fe at the hollow site, due to the different electronic solution previously discussed.

To inspect the effect of the Ni(111) substrate on the LDOS we show in Fig. 5 the LDOS of Co/G/Ni(111) at the fcc adsorption site. The comparison with Fig. 1 for the corresponding unsupported case reveals that the LDOS is rather similar in terms of peak positions (peaks associated with  $d$  states are located at the same energies), but some difference in width (broadening) exists, e.g., of the  $d_{z^2}$  symmetry orbital. A full account of the LDOS for all elements and adsorption sites can be found in Figs. S6– S13 in Ref. [43]). More notably, the  $s$  orbital peaks in the supported system get broadened due to hybridization with the Ni substrate through the mediation

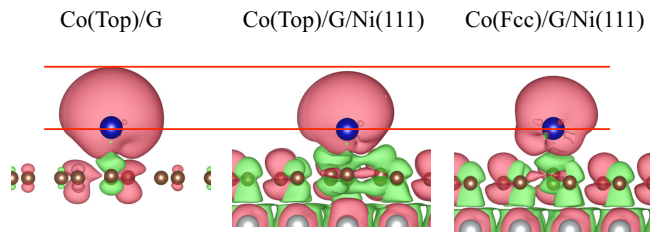


FIG. 6. Spin-polarized charge density isosurfaces (isovalue of 0.0005) of Co adatom for the top/G (left), top/G/Ni(111) (center), and fcc/G/Ni(111) (left) cases. Color code is as follows: Red (dark gray) and green (light gray) indicate positive and negative magnetization. Red lines are guides to the eyes.

of the graphene layer. The  $s$  electron which contributes to the  $d^{n+1}s^1$  solution becomes therefore less localized on the adatom, and this delocalization is accompanied by a reduction of the  $s$  spin polarization. Band structure analysis (see Fig. S14 in Ref. [43]) confirms the localized nature of the spin-polarized  $s$  orbital and its partial quenching moving from G to G/Ni.

We can visualize this by plotting in Fig. 6 isosurfaces of the three-dimensional spin polarized charge density on Co, for the top site on graphene (left panel) and top and fcc sites on G/Ni(111) substrates (center and right panel, respectively). The spherical spin density hat above the Co adatom, hosted by the  $s$  orbital, is clearly visible for Co on unsupported graphene, and is partly quenched in the presence of the Ni substrate. Thus, although the spin moment integrated on the  $d$  orbitals is only slightly modified (see Tables II and III), the total spin on the adatom is indeed influenced by the interaction with the Ni substrate. This behavior is found to be common for all the adatoms across the 3d TM series, and holds for both hollow and top/fcc adsorption sites.

## V. CONCLUSIONS

We have presented a thorough computational analysis by DFT calculations of the structural, electronic, and magnetic properties of isolated 3d transition metal adatoms adsorbed on unsupported graphene and on graphene/Ni(111) substrates. The different levels of interaction with the adatoms that characterize the two substrates lead to modifications which are relevant especially at the end of the TM series. A change in the preferred adsorption site is observed for Fe and Co adatoms due to the presence of the Ni substrate: Fe and Co are preferentially adsorbed on hollow sites in free-standing geometry, whereas in the Ni-supported setup both adatoms adsorb more favorably on the fcc site. The electronic and magnetic states of the adatoms are found to be only mildly modified by the presence of the Ni substrate below graphene, although a partial quenching of the spin polarization residing in the  $s$  orbitals is observed throughout the series. The magnetic coupling between the adatom spin and the Ni magnetization is found to vary sensibly in sign and size as a function of the adatom element and of the occupied adsorption site. When considering the lowest energy adsorption site, our data suggest that the exchange coupling is antiferromagnetic (antiparallel spin alignment) at the beginning of the series (from Ti to Cr) and ferromagnetic (parallel spin alignment) at the end of the series (from Mn to Co).

## ACKNOWLEDGMENTS

Computation time at the CINECA supercomputing center through the ISCRA initiative and at the Vienna Scientific Cluster (VSC) is gratefully acknowledged. Fruitful discussions with Dr. Jindrich Kolorenc, Dr. Alessandro Barla, Dr. Sergii Khmelevskyi, and Dr. Alexander Shick are also acknowledged.

- [1] H. Brune and P. Gambardella, *Sur. Sci.* **603**, 1812 (2009).
- [2] A. A. Khajetoorians, J. Wiebe, B. Chilian, S. Lounis, S. Blügel, and R. Wiesendanger, *Nat. Phys.* **8**, 497 (2012).
- [3] I. G. Rau, S. Baumann, S. Rusponi, F. Donati, S. Stepanow, L. Gragnaniello, J. Dreiser, C. Piamonteze, F. Nolting, S. Gangopadhyay *et al.*, *Science* **344**, 988 (2014).
- [4] H. T. Dang, M. dos Santos Dias, A. Liebsch, and S. Lounis, *Phys. Rev. B* **93**, 115123 (2016).
- [5] F. D. Natterer, K. Yang, W. Paul, P. Willke, T. Choi, T. Greber, A. J. Heinrich, and C. P. Lutz, *Nature (London)* **543**, 226 (2017).
- [6] F. Donati, S. Rusponi, S. Stepanow, C. Wäckerlin, A. Singha, L. Persichetti, R. Baltic, K. Diller, F. Patthey, E. Fernandes *et al.*, *Science* **352**, 318 (2016).
- [7] G. Avvisati, C. Cardoso, D. Varsano, A. Ferretti, P. Gargiani, and M. G. Betti, *Nano Lett.* **18**, 2268 (2018).
- [8] H. Sevinçli, M. Topsakal, E. Durgun, and S. Ciraci, *Phys. Rev. B* **77**, 195434 (2008).
- [9] H. Valencia, A. Gil, and G. Frapper, *J. Phys. Chem. C* **114**, 14141 (2010).
- [10] T. O. Wehling, A. I. Lichtenstein, and M. I. Katsnelson, *Phys. Rev. B* **84**, 235110 (2011).
- [11] T. Zhang, L. Zhu, S. Yuan, and J. Wang, *Chem. Phys. Chem.* **14**, 3483 (2013).
- [12] M. Manadé, F. Vines, and F. Illas, *Carbon* **95**, 525 (2015).
- [13] E. del Castillo, F. Cargnoni, R. Soave, and M. I. Trioni, *Phys. Scr.* **91**, 053007 (2016).
- [14] N. Dimakis, F. A. Flor, A. Salgado, K. Adjibi, S. Vargas, and J. Saenz, *Appl. Sur. Sci.* **421**, 252 (2017).
- [15] Y. Virgus, W. Purwanto, H. Krakauer, and S. Zhang, *Phys. Rev. B* **86**, 241406(R) (2012).
- [16] A. N. Rudenko, F. J. Keil, M. I. Katsnelson, and A. I. Lichtenstein, *Phys. Rev. B* **86**, 075422 (2012).
- [17] Y. Virgus, W. Purwanto, H. Krakauer, and S. Zhang, *Phys. Rev. Lett.* **113**, 175502 (2014).
- [18] R. Mozara, M. Valentyuk, I. Krivenko, E. Şaşıoğlu, J. Kolorenc, and A. I. Lichtenstein, *Phys. Rev. B* **97**, 085133 (2018).
- [19] T. O. Wehling, H. P. Dahal, A. I. Lichtenstein, M. I. Katsnelson, H. C. Manoharan, and A. V. Balatsky, *Phys. Rev. B* **81**, 085413 (2010).
- [20] D. Jacob and G. Kotliar, *Phys. Rev. B* **82**, 085423 (2010).
- [21] J. Ren, H. Guo, J. Pan, Y. Y. Zhang, X. Wu, H.-G. Luo, S. Du, S. T. Pantelides, and H.-J. Gao, *Nano Lett.* **14**, 4011 (2014).

- [22] F. Donati, Q. Dubout, G. Autès, F. Patthey, F. Calleja, P. Gambardella, O. V. Yazyev, and H. Brune, *Phys. Rev. Lett.* **111**, 236801 (2013).
- [23] T. Eelbo, M. Waśniowska, M. Gyamfi, S. Forti, U. Starke, and R. Wiesendanger, *Phys. Rev. B* **87**, 205443 (2013).
- [24] T. Eelbo, M. Waśniowska, P. Thakur, M. Gyamfi, B. Sachs, T. O. Wehling, S. Forti, U. Starke, C. Tieg, A. I. Lichtenstein *et al.*, *Phys. Rev. Lett.* **110**, 136804 (2013).
- [25] F. Donati, L. Gragnaniello, A. Cavallin, F. D. Natterer, Q. Dubout, M. Pivetta, F. Patthey, J. Dreiser, C. Piamonteze, S. Rusponi *et al.*, *Phys. Rev. Lett.* **113**, 177201 (2014).
- [26] B. Kiraly, A. N. Rudenko, W. M. J. van Weerdenburg, D. Wegner, M. I. Katsnelson, and A. A. Khajetoorians, *Nat. Commun.* **9**, 3904 (2018).
- [27] S. Marocchi, P. Ferriani, N. M. Caffrey, F. Manghi, S. Heinze, and V. Bellini, *Phys. Rev. B* **88**, 144407 (2013).
- [28] A. Candini, V. Bellini, D. Klar, V. Corradini, R. Biagi, V. D. Renzi, K. Kummer, N. B. Brookes, U. del Pennino, H. Wende *et al.*, *J. Phys. Chem. C* **118**, 17670 (2014).
- [29] A. Candini, D. Klar, S. Marocchi, V. Corradini, R. Biagi, V. De Renzi, U. del Pennino, F. Troiani, V. Bellini, S. Klyatskaya *et al.*, *Sci. Rep.* **6**, 21740 EP (2016).
- [30] S. Marocchi, A. Candini, D. Klar, W. Van den Heuvel, H. Huang, F. Troiani, V. Corradini, R. Biagi, V. De Renzi, S. Klyatskaya *et al.*, *ACS Nano* **10**, 9353 (2016).
- [31] P. Ferriani, S. Heinze, and V. Bellini, *Sci. Rep.* **7**, 3647 (2017).
- [32] V. Karpan, G. Giovannetti, P. Khomyakov, M. Talanana, a. Starikov, M. Zwierzycki, J. van den Brink, G. Brocks, and P. Kelly, *Phys. Rev. Lett.* **99**, 176602 (2007).
- [33] O. V. Yazyev and A. Pasquarello, *Phys. Rev. B* **80**, 035408 (2009).
- [34] K. K. Saha, A. Blom, K. S. Thygesen, and B. K. Nikolić, *Phys. Rev. B* **85**, 184426 (2012).
- [35] D. Kim, A. Hashmi, C. Hwang, and J. Hong, *Appl. Phys. Lett.* **102**, 112403 (2013).
- [36] G. Kresse and J. Furthmüller, *Phys. Rev. B* **54**, 11169 (1996).
- [37] G. Kresse and D. Joubert, *Phys. Rev. B* **59**, 1758 (1999).
- [38] J. P. Perdew, K. Burke, and M. Ernzerhof, *Phys. Rev. Lett.* **77**, 3865 (1996).
- [39] S. Grimme, *J. Comput. Chem.* **27**, 1787 (2006).
- [40] P. Janthon, F. Viñes, S. M. Kozlov, J. Limtrakul, and F. Illas, *J. Chem. Phys.* **138**, 244701 (2013).
- [41] A. I. Lichtenstein, V. I. Anisimov, and J. Zaanen, *Phys. Rev. B* **52**, R5467 (1995).
- [42] G. Jomard, B. Amadon, F. Bottin, and M. Torrent, *Phys. Rev. B* **78**, 075125 (2008).
- [43] See Supplemental Material at <http://link.aps.org/supplemental/10.1103/PhysRevMaterials.5.014406> for Schematic view of the top-fcc and bridge top stacking of G/Ni(111); Adopted computational protocol to seek the GGA+U ground state; Analysis of the role of VdW interaction; Relation between Bader charges and adatom-G equilibrium distances; Discussion on orbital occupation and magnetic moments; Spin density analysis for the hollow site adsorption; LDOS plots for the whole set of calculations; Band structure analysis for Co on hollow site on G and G/Ni substrates.
- [44] W. Zhao, S. M. Kozlov, O. Hofert, K. Gotterbarm, M. P. A. Lorenz, F. Vines, C. Papp, A. Gorling, and H.-P. Steinrück, *J. Phys. Chem. Lett.* **2**, 759 (2011).
- [45] A. Barla, V. Bellini, S. Rusponi, P. Ferriani, M. Pivetta, F. Donati, F. Patthey, L. Persichetti, S. K. Mahatha, M. Papagno *et al.*, *ACS Nano* **10**, 1101 (2016).
- [46] G. Henkelman, A. Arnaldsson, and H. Jónsson, *Comp. Mater. Science* **36**, 354 (2006).
- [47] V. Sessi, S. Stepanow, A. N. Rudenko, S. Krotzky, K. Kern, F. Hiebel, P. Mallet, J.-Y. Veuillen, O. Šipr, J. Honolka *et al.*, *New J. Phys.* **16**, 062001 (2014).
- [48] M. Afshar and M. Hemati, *Phys. Lett. A* **382**, 3476 (2018).
- [49] M. Weser, Y. Rehder, K. Horn, M. Sicot, M. Fonin, A. B. Preobrajenski, E. N. Voloshina, E. Goering, and Y. S. Dedkov, *Appl. Phys. Lett.* **96**, 012504 (2010).
- [50] C. F. Hermanns, K. Tarafder, M. Bernien, A. Krüger, Y.-M. Chang, P. M. Oppeneer, and W. Kuch, *Adv. Mater.* **25**, 3473 (2013).
- [51] D. Klar, S. Bhandary, A. Candini, L. Joly, P. Ohresser, S. Klyatskaya, M. Schleberger, M. Ruben, M. Affronte, O. Eriksson *et al.*, *Phys. Rev. B* **89**, 144411 (2014).
- [52] M. Vanin, J. J. Mortensen, A. K. Kelkkanen, J. M. Garcia-Lastra, K. S. Thygesen, and K. W. Jacobsen, *Phys. Rev. B* **81**, 081408 (2010).
- [53] M. Gao, Y. Pan, C. Zhang, H. Hu, R. Yang, H. Lu, J. Cai, S. Du, F. Liu, and H.-J. Gao, *Appl. Phys. Lett.* **96**, 053109 (2010).
- [54] A. Dahal, R. Addou, H. Coy-Diaz, J. Lallo, and M. Batzilla, *APL Mater.* **1**, 042107 (2013).
- [55] A. Tamtögl, E. Bahn, J. Zhu, P. Fouquet, J. Ellis, and W. Allison, *J. Phys. Chem. C* **119**, 25983 (2015).
- [56] A. B. Preobrajenski, M. L. Ng, A. S. Vinogradov, and N. Mårtensson, *Phys. Rev. B* **78**, 073401 (2008).
- [57] A. Varykhalov, J. Sánchez-Barriga, A. M. Shikin, C. Biswas, E. Vescovo, A. Rybkin, D. Marchenko, and O. Rader, *Phys. Rev. Lett.* **101**, 157601 (2008).
- [58] A. M. Shikin, V. K. Adamchuk, and K. H. Rieder, *Phys. Solid State* **51**, 2390 (2009).
- [59] M. Hasegawa, K. Nishidate, T. Hosokai, and N. Yoshimoto, *Phys. Rev. B* **87**, 085439 (2013).
- [60] C. S. Praveen, S. Piccinin, and S. Fabris, *Phys. Rev. B* **92**, 075403 (2015).
- [61] V. Corradini, A. Candini, D. Klar, R. Biagi, V. De Renzi, A. Lodi Rizzini, N. Cavani, U. del Pennino, S. Klyatskaya, M. Ruben *et al.*, *Nanoscale* **10**, 277 (2018).
- [62] S. Bhandary, S. Ghosh, H. Herper, H. Wende, O. Eriksson, and B. Sanyal, *Phys. Rev. Lett.* **107**, 257202 (2011).
- [63] The electronic occupation computed by VASP results from an integration over the Wigner-Seitz sphere of the charge density; in case of extended orbitals as the one with *s* or *p* symmetries, a large part of the density leaks out and is not accounted for in such integration. Note that this holds also if the *s* orbital is fully occupied. In order to supply a plot where the occupation of the *d* and *s* electron can be qualitatively compared to each other we have normalized the data according to the following criteria: the integral over the full and empty LDOS (that also comes from a spatial integration over the energy resolved charge density over the Wigner-Seitz sphere) of the *d* orbitals is normalized to 5 (for each spin channel) and, similarly, the one on the *s* LDOS is normalized to 1. In this way we can visually (and qualitatively) follow the progressive occupation of the orbitals with different symmetries for the different elements of the 3*d* series.